Mohamed A. Abbas* and Mahmoud A. Bedair

Adsorption and Computational Studies for Evaluating the Behavior of Silicon Based Compounds as Novel Corrosion Inhibitors of Carbon Steel Surfaces in Acidic Media

https://doi.org/10.1515/zpch-2018-1159
Received February 17, 2018; accepted April 7, 2018

Abstract: Two organo-silicon compounds namely; di-triethanolamine siloxane and bis (dithioamine triethanolamine) siloxane were employed as inhibitors for C-steel alloys corrosion in 1 M H_2SO_4 solution utilizing potentiodynamic polarization, electrochemical impedance and computational studies. According to both polarization and impedance data, it has been found that the investigated organo-silicon compounds work as efficient corrosion inhibitors and the protection aptitude raised by increasing the inhibitor concentration. The shown behavior of the tested compounds is cathodic and anodic type inhibition following Langmuir's adsorption isotherm. The evaluated adsorption parameters, adsorption equilibrium constant (K_{ads}) and Gibbs free energy of adsorption (ΔG^o_{ads}) reveal a good association between the inhibitor molecules and the surface of carbon steel in a predominantly chemisorptions manner. In the view of computational quantum and molecular dynamic simulation studies, molecular structure effectiveness and suggested mechanism of protection efficiency were discussed. Surface characterization studies such as scanning electron microscopy (SEM), energy dispersive X-ray (EDX) and X-ray diffraction (XRD) have been utilized as corroborative tools for confirming the presence of the defensive inhibitor film on the surface of a metal.

Keywords: acidic inhibition; carbon steel; computational studies; polarization; siloxane derivatives.

***Corresponding author: Mohamed A. Abbas,** Petroleum Applications Department, Egyptian Petroleum Research Institute (EPRI), Nasr City, P.B. 11727, Cairo, Egypt,
Tel.: +20 2 22745902, Fax: +20 2 22747433, e-mail: mohamedabbas1966@yahoo.com
Mahmoud A. Bedair: Chemistry Department, Faculty of Science (Men's Campus), Al-Azhar University, Nasr City, P.B. 11884, Cairo, Egypt

1 Introduction

Alloys of steel are utilized in great quantities in processing of chemicals, petroleum extraction as well as refining, building and metal processing equipments. These applications usually cause severe corrosive effects on equipment's [1]. Corrosion has tremendous negative economic effects and therefore the search for long-lasting and effective inhibitors, which protect carbon steel surfaces [2]. Utilization of corrosion inhibitors is a standout amongst the generality efficient and feasible techniques for commanding corrosion process especially in acid electrolytes to limit unexpected steel dissolution in addition acid depletion [3]. The greater of the corrosion inhibitors restrain corrosion due to the adsorption of inhibitor molecules on the surface of metal. Factors affecting the behavior of adsorption are; inhibitor nature, a metal surface state and excess charge from metal surface [4]. Most of the widely-known acidic corrosion inhibitors are organic compounds, especially those containing sulfur, nitrogen or oxygen particles [5]. Generally the nitrogen, sulfur, and oxygen compounds which contain unsaturated π-bonds, planar and conjugated aromatic rings are of exceptional avails in order to they could be with ease adsorbed at the surface by means of the variable adsorption focuses [6]. Nowadays, organosilane chemistry is enabling the development of novel, more environmentally safe technologies for corrosion protection. Organosilane chemistry provides a wide variety of benefits to coatings. Silanes are been utilized recently like a green pre-treatment film for metals like steel, aluminum, copper and their alloys, with a view to improve the cohesion of several organic coatings [7]. Silanes are promising materials because the films of silane have chemically steady and can form homogeneous layers which acting as a successful effective obstruction against oxygen dissemination and chemical assault [8]. However, in addition to surface treatment/coating, Siloxanes could be used as an inhibition for protecting metals alloys and metals from corrosion attack. The efficiency from corrosion inhibitions is directly related to the quality of the functional groups included in the structure of the compound, spatial molecular structure, the structure of the molecular electronic, and the surface nature of metal. Siloxanes are considered as a high-efficiency inhibitor in corrosion process due to the being of π-bonds and hetero-compounds contain heteroatoms like nitrogen, sulfur, and oxygen which enhance the effectiveness of these compounds [9, 10]. Recently good trends to the corrosion processes study are combining the experimental data together with theoretical molecular studies [11]. Molecular dynamic simulation and quantum chemical calculation have proposed as effective and fast means to help in the interpretations of experimental results. In addition, theoretical calculations can cast light on the correlation of the electronic peculiarity and the corrosion inhibitors performance [12].

Our work is focused on the investigation of the effectiveness of two novel organo-silicon compounds as corrosion inhibitions with regard to carbon steel in 1 M H_2SO_4 by electrochemical techniques and the results were confirmed by surface study. Adsorption parameters of the thermodynamic are studied and debated in specifics and also, both computational quantum and molecular dynamic simulation studies, have further utilized to analyze the adsorption energies of the prepared compounds upon alloy surface and to assist in the interpretation of the experimental results.

2 Methodology of experimental work

2.1 Assembly of organo-silicon components

The organo-silicon compounds; di-triethanolamine siloxane (compound I) and bis dithioamine triethanolamine siloxane (compound II) which are examined as corrosion inhibitors were synthesized according to our previous experimental work [10]. The products were purified and described by using infra-red, proton nuclear magnetic resonance spectroscopy and elemental analysis. The molecular structure of new organo-silicon compounds is displayed in Figure 1.

2.2 Used materials and solutions

The chemical composition of carbon steel which it was conducted the electrochemical experiments has (wt.%): 0.19% C, 0.05% Si, 0.94% Mn, 0.009% P, 0.004% S, 0.014% Ni, 0.009% Cr, 0.034% Al, 0.016% V, 0.003% Ti, 0.022% Cu, and the remainder Fe. The analytical grade sulfuric acid (H_2SO_4) (E. Merck) was

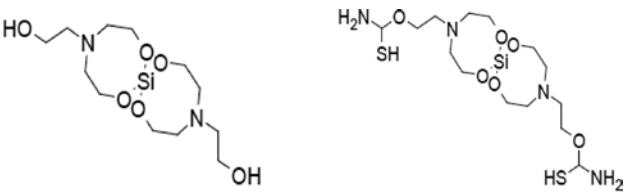

Fig. 1: The molecular structure of the synthesized organo-silicon compounds.

diluted to 1 molar sulfuric acid (1 M H_2SO_4) by utilizing bi-distilled water, which has used as the corrosive electrolyte. The prepared compounds have been applied at concentrations ranging from 0.000001 to 0.01 M/L.

2.3 Electrochemical measurements

The gauge of electrochemical polarization and impedance were carried out by using Volta-lab apparatus, (PGZ 301 – France), which potentiostat dominated by utilized appraisal of corrosion software version (Volta-lab 4) under constant conditions. A conventional electrochemical cell consists of working electrode (carbon steel), an auxiliary electrode (platinum) and reference electrode saturated calomel (SCE) was established during experiments implementation. The surface of carbon steel (1 cm^2) have been prepared on four steps; abrading by using various emery papers (320→1200), washing by distilled water, rinsing by acetone, and finally drying.

Prior to electrochemical spectroscopic measurements, a steel specimen has left in 1 M H_2SO_4 solution for 30 min to get steady state. Curves of Tafel have been performed by modifying the potential of electrode (from –800 to –300 mV vs. SCE) with a scan rate of 2 mV s^{-1}.

EIS measurements which are nondestructive technique based on AC current were conducted in the scope of frequencies starting from 100 kHz and ending at 50 mHz.

A signal with 10 mV amplitude utilized to upset the system. Zsimpwin program was used to evaluate the data collected from EIS measurements.

2.4 Surface examination studies

The coupons of carbon steel were immersed in various solutions (uninhibited and inhibited ones) for a period of 24 h to get insights about the morphological and structural changes occurred on the surface. The morphology and structural ease of the formed layer on the surface of the coupons were analyzed by SEM, EDX and XRD.

The scan electron microscope images were conducted using JEOL model JSM-5400. Elemental analysis of the formed layer on the surface of coupons before and after applying the inhibitors was performed using EDX analysis. The identification of the corrosion product phases covering the surface of the coupons were realized by using X-ray powder diffractometer, X'PERT PRO MPD (PANalytical, the Netherland). The XRD patterns were recorded with a Cu Kα radiation of

wavelength of 1.54 Å operated at 40 kV/40 mA. The coupons were step-scanned in the 2θ range of 4–80° with a step size 0.02 and a time step of 0.4 s. The singular crystalline phases formed on the carbon steel surface were known by utilizing the ICDD-PDF database.

2.5 Quantum chemical studies

Quantum chemical calculation of compound I and compound II was performed firstly by PM6 semi-empirical. Density functional theory (DFT) [13], at B3LYP/6-31G+ (d,p) basis set [14, 15] and Hartree–Fock method (HF) utilizing 6-31G+ (d,p) basis set. The obtained structures were used for re-optimizing the chemical structures of the studied compounds [16]. Dawning tools by Gauss View, 5.0 and Gaussian 09 software were used for constructing and optimizing the chemical structures of compound I and compound II [17]. The quantum chemical parameters including potential of ionization, I, affinity of electron, A, Absolute electro negativity, X, absolute hardness, η, chemical potential, μ, global electrophilicity power [18], ω, and fraction of electron transferred [19], ΔN, are calculated by using the following equations:

$$I = -E_{\text{HOMO}},\ A = -E_{\text{LUMO}} \tag{1}$$

$$\chi = (I + A)/2,\ \chi = -[(E_{\text{LUMO}} + E_{\text{HOMO}})/2] \tag{2}$$

$$\eta = (I - A)/2,\ \eta = -[(E_{\text{LUMO}} - E_{\text{HOMO}})/2] \tag{3}$$

$$\mu = -\chi,\ \omega = \mu^2/2\eta,\ \Delta N = (\chi_{\text{Fe}} - \chi_{\text{inh}})/2(\eta_{\text{Fe}} + \eta_{\text{inh}}) \tag{4}$$

2.6 Molecular dynamics simulations

The configuration of organo-silicon inhibitors (compounds I and II) on steel surface were studied by the Adsorption Locator module of the Materials studio 4.3 software from Accelrys Inc. [20]. Drawing tools in visualized materials are used to build inhibitor molecules as well as steel surface. The steel surface was represented by Fe crystal. The First step was cleaving crystal along the (110) plane, as it is the greatest stable surface [21]. Secondly the plane was expanded into a suitable super-cell to accommodate an extended surface. The interplay between compound I, compound II and Fe surface was assumed in an emulation box (22.90 Å × 57.26 Å × 26.68 Å) with periodic border circumstances. Iron sheet of

6.00 Å and a vacuum layer of 15.00 Å heights are the components of the box. The interaction energy $E_{\text{Fe–inhib.}}$ was intended by the following equation:

$$E_{\text{Fe–inhib.}} = E_{\text{complex}} - (E_{\text{Fe}} + E_{\text{inhib.}}) \tag{5}$$

where, E_{complex} represents the entire energy of Fe crystal together with the adsorbed inhibitor molecule. E_{Fe} and $E_{\text{inhib.}}$ are the entire energy of Fe crystal and free inhibitor molecules, respectively. The binding energy was the negative sign value of an interplay energy as follows:

$$E_{\text{binding}} = -E_{\text{Fe–inhibitor}}. \tag{6}$$

3 Results and discussion

3.1 Polarization curves

In order to investigate the effect of adding different concentrations of the investigated compounds (I and II) on anodic C-steel oxidation and so cathodic hydrogen reduction, potentiodynamic polarization were done. Typical potentiodynamic without and with different concentration of compounds I and II are presented in Figure 2, while the electrochemical parameters obtained from Tafel's polarization curves are collected in Table 1. Adding several concentrations of both compounds I and II has a remarkable effect on both anodic and cathodic partial reactions. It is clear from data that the corrosion potential (E_{corr}) has been shifted a bit towards more positive (anodic) values in the existence of compounds I and II. Additionally, it is noted that the cathodic current densities and so the corrosion current density (i_{corr}) had been reduced in the existence of the investigated compounds. Usually inhibitors of corrosion can be considered as an anodic or cathodic type if the displacement in value of E_{corr} is more than 85 mV [22]. Inspection of Table 1, it is clear that a slight change is noticed in the potential of corrosion after the addition of the tested inhibitors with respect to blank solution (carbon steel in 1 M H_2SO_4), suggesting a mixed-type behavior in 1 M H_2SO_4. Another key fact to remember is Table 1 shows that the decrease in values of corrosion current density is accompanied by an increase in inhibitor concentrations, which leads to that the inhibition efficiencies increase by increasing inhibitors concentrations. This is a result of forming of protective layers of tested inhibitors on carbon steel surface by a simple surface-blocking mechanism, as the inhibitor adsorbed firstly on steel surface and then reduce the corrosion current density by blocking the available corrosion reaction active sites [23].

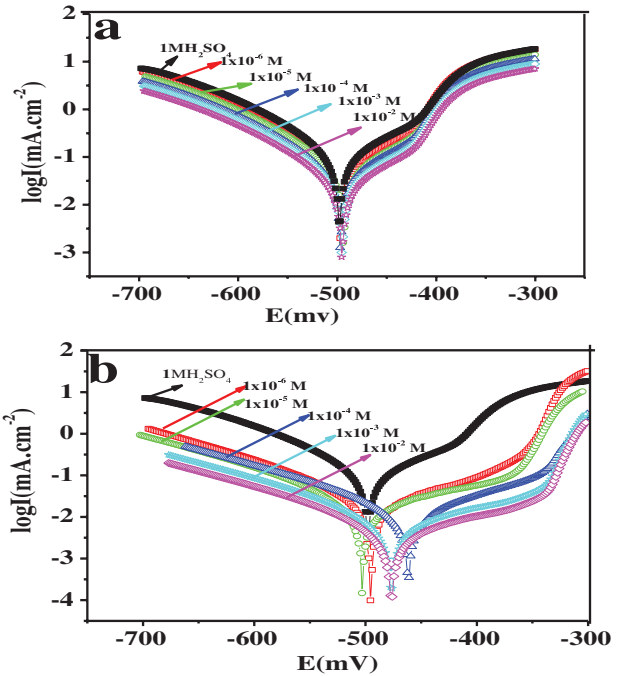

Fig. 2: Tafel polarization curves for the carbon steel in 1 M H_2SO_4 in the absence and presence of different concentrations of (a) compound I and (b) compound II.

Tab. 1: Electrochemical polarization parameters for the carbon steel in 1 M H_2SO_4 with and without addition of different concentrations of the investigated compounds.

Inhibitors	C×10⁵ (M)	E_{corr} (mV/SCE)	I_{corr} (mA/cm²)	Rp (Ω cm²)	β_a (mV/dec)	β_c (mV/dec)	θ	η%
Compound I	Blank	−497.8	0.465	49.00	83.5	−174.0	–	–
	0.1	−494.3	0.136	229.9	72.2	−109.5	0.707	71
	1	−496.4	0.127	246.2	71.7	−107.9	0.727	73
	10	−496.5	0.123	250.0	71.4	−107.6	0.735	74
	100	−495.1	0.104	243.1	67.8	−98.3	0.776	78
	1000	−493.6	0.100	253.5	66.7	−98.5	0.785	79
Compound II	Blank	−497.8	0.465	49.00	83.50	−174.0	–	–
	0.1	−495.4	0.037	1090	65.80	−129.1	0.920	92
	1	−503.0	0.035	1410	79.80	−139.7	0.925	93
	10	−461.6	0.016	1970	161.5	−133.2	0.965	97
	100	−482.9	0.012	2420	186.6	−124.7	0.974	97
	1000	−467.8	0.011	2900	166.1	−134.0	0.976	98

3.2 Electrochemical impedance spectroscopy

The kinetics of the electrochemical processes and the capacitive behavior of the synthesized inhibitors for carbon steel are being characterized via EIS measurements. The carbon steel Nyquist plots in 1 M H_2SO_4 with and without investigated compounds are offered in Figure 3. It can be noted from the Figure that all the spectra of impedance acquired a solitary, slightly engaged semi-circle, elucidating a lack of perfect capacitive demeanor of the solid/liquid interface controlled electrochemically. The frequency dispersing effect phenomenon is said to be attained at this stage and it is commonly results from electrode surface roughness and heterogeneity [24]. Over and above, the capacitive loops diameter are larger in the inhibitor existence than in its non-attendance (blank solution) and it raises pointedly accompanied by increasing inhibitor concentration, which can be linked to the increase in surface coverage which achieved by adsorption of inhibitor molecules on the carbon steel surface and signalizes that the charge transfer process mainly, responsible for the carbon steel corrosion control.

In accordance with the above results, an equivalent circuit model R (QR) was applied to simulate and suit the experiential EIS results. The circuit contains

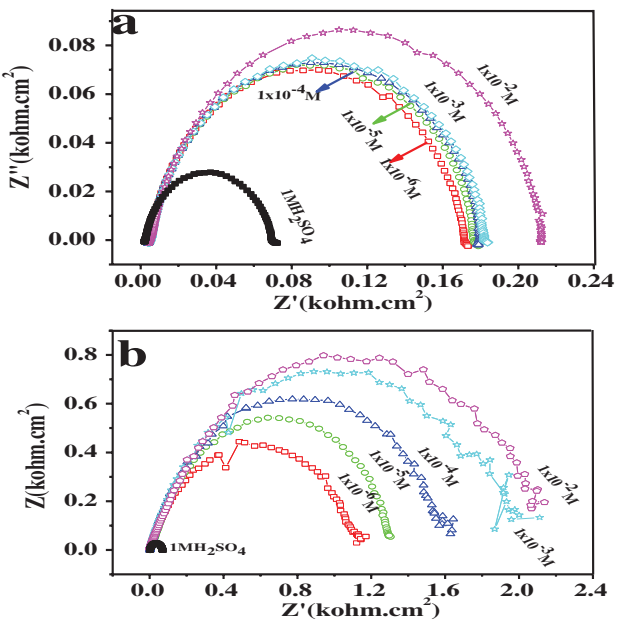

Fig. 3: Impedance curves for the carbon steel in 1 M H_2SO_4 in the absence and presence of different concentrations of (a) compound I and (b) compound II.

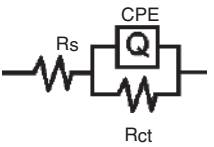

Fig. 4: Equivalent circuit diagram used to simulate and fit all impedance data.

electrolyte resistance (R_s), charge transfer resistance (R_{ct}) and constant phase element (CPE) as shown in Figure 4. So as to obtain a more exact fitting to the experimental data the CPE is utilized instead of double layer capacitance (C_{dl}) and it is comprised a component (Q) and a coefficient (n) that determines diverse physical phenomena like surface heterogeneity resulting from surface roughness, inhibitor adsorption, porous layer formation and degree of polycrystallinity. The CPE impedance function is represented by the following expression [25]:

$$Z_{CPE} = Y_o^{-1}(j\omega)^{-n} \tag{7}$$

where, Y_o is the factor of proportionality; ω is the angular frequency ($\omega = 2\pi f$, the frequency in Hz); j is the imaginary unit and, n the variation parameter ($-1 \le n \le +1$), has the indication of a phase shift and giving insights about the surface inhomogeneity degree. If $n = 0$, the CPE signifies a pure resistor, for $n = -1$ and inductor and for $n = +1$, a pure capacitor. The values of the double layer capacitance (Q) and inhibition efficiency (η_E) are calculated as follows:

$$Q = Y_o(\omega_m^n)^{n-1} \tag{8}$$

$$\eta_{EIS}(\%) = \frac{R_{ct} - R_{ct}^o}{R_{ct}} \times 100 \tag{9}$$

where, ω_m^n is the angular frequency at the maximum value of the imaginary part of the impedance spectrum. R_{ct}^o and R_{ct} are the charge transfer resistance in the absence and presence of organo-silicon compound inhibitors, respectively.

As offered in Table 2, the value of R_{ct} increases predominantly by increasing inhibitor concentration of both compounds I and II, while the values of Q are brought down. It is clearly observed from Table 2 that, R_{ct} of inhibited system increased from 70 Ω cm^2 (blank solution) to 209 and 2165 Ω cm^2 and double layer capacitance C_{dl} decreased from 148 μFcm^{-2} (inhibitor free solution) to 98 and 44 μFcm^{-2} in the occurrence of maximum concentration of compound I and II, respectively. A slower corroding system is escorted with large charge transfer resistance. In contrast, better protection given by an inhibitor is correlated with the decreasing of the metal capacitance. According to the well known Helmholtz model [26]:

Tab. 2: Impedance parameters for the carbon steel in 1 M H_2SO_4 solution with and without addition of different concentrations of organo-silicon compounds.

Medium	C×10⁵ (M)	R_s (Ω cm²)	Q×10⁵ (Q/S sⁿ cm⁻²)	n	R_{ct} (Ω cm²)	C_{dl} (μFcm⁻²)	θ	η%
Compound I	Blank	4.775	48.99	0.870	70	148	–	–
	0.1	3.650	17.2	0.885	168	129	0.583	58.3
	1	5.320	22.4	0.865	175	114	0.600	60.0
	10	6.250	19.9	0.871	177	113	0.604	60.4
	100	4.989	19.7	0.870	179	105	0.608	60.8
	1000	5.030	17.7	0.860	209	98	0.665	66.5
Compound II	Blank	4.775	48.99	0.87	70	148	–	–
	0.1	2.25	6.739	0.85	1134	59.0	0.938	93.8
	1	10.69	9.580	0.80	1306	50.0	0.946	94.6
	10	2.69	6.820	0.84	1618	48.5	0.957	95.7
	100	0.87	7.230	0.82	2020	49.0	0.965	96.5
	1000	4.69	8.360	0.80	2165	44.0	0.968	96.8

$$C_{\mathrm{dl}} = \frac{\varepsilon_o \varepsilon a}{t} \tag{10}$$

where, t is the protective layer thickness, ε_o is the air permittivity, ε is the local dielectric constant and a is the electrode surface area. The decrease in Q is a reflection of either a rebate in the local dielectric constant or an elevation in the electrical double layer thickness, suggested that inhibitor molecules adsorbed at the metal/acid interface thereby suppress the iron corrosion. Hence, upon addition of compounds I and II, their adsorption takes place on the electrode surface willingly with the water molecules replacing. The data obtained show that, the values of R_{ct} comply with the arrangement of II > I and the values of Q follow the order of II < I, leading to the protection efficiency order: II > I, all of them at the same concentration. The maximum values of performance efficiency are 96.8% and 66.5% for compounds II and I, respectively. These results show that compound II is more efficacious to rein the corrosion of C-steel in 1 M H_2SO_4 solution than compound I.

3.3 Thermodynamic considerations based on adsorption isotherm

If any organic compound is able to fetch adsorbed on the steel surface via involving the replacement of the water molecules at the corroding surface, this

compound is termed as an efficient and a felicitous corrosion inhibitor due to its adsorption ability according to the following equation [27]:

$$OI_{(aq.)} + n\ H_2O_{(ads)} \rightarrow OI_{(ads)} + H_2O_{(aq.)} \tag{11}$$

where, $OI_{(sol)}$ and $OI_{(ads)}$ are the organic inhibitor molecules studied in the solutions and adsorbed on the carbon steel surface, respectively, and the size ratio which is, the number of water molecules replaced by the organic molecules, is symbolized as n.

To fulfill the nature of the adsorption mode of the studied inhibitors, the surface coverage data (θ) as a function of inhibitor concentration was calculated from the corrosion current densities obtained from polarization results at 303 K using the following equation:

$$\theta = \frac{I_{\text{uninh.}} - I_{\text{inh.}}}{I_{\text{uninh.}}} \tag{12}$$

where, $I_{\text{uninh.}}$ and $I_{\text{inh.}}$ are the corrosion current densities in the lack and occurrence of the inhibitors, respectively. The (η%) of the surfactants is calculated by the following equation [28].

$$\eta\% = \frac{I_{\text{uninh.}} - I_{\text{inh.}}}{I_{\text{uninh.}}} \times 100 \tag{13}$$

An attempt has been applied to fit theoretically the values of surface coverage (θ) into different adsorption isotherm models like Langmuir, Temkin, and Frumkin. Among them, The Langmuir adsorption isotherms were found to provide the optimum fitting for the adsorption tendency of the studied inhibitors based on the values of the correlation coefficients (R^2) as presented in Table 3. Detailed experimental data were graphically represented in Figure 5 by plotting C_{inh}/θ versus C_{inh} according to the following equations, basic and rearranged one which are describing the Langmuir adsorption isotherm [29]:

Tab. 3: Different thermodynamic parameters of the linear regression C_{inh}/θ and C_{inh} in 1 M H_2SO_4 for the two scrutinized compounds I and II at room temperature.

Inhibitors	Parameters			
	Regression coefficient (R^2)	Slope	K_{ads} ($M^{-1} \times 10^4$)	ΔG (kJ mol^{-1})
Compound I	1.0	1.2734	16.56	−40.4
Compound II	1.0	1.0245	104.2	−45.0

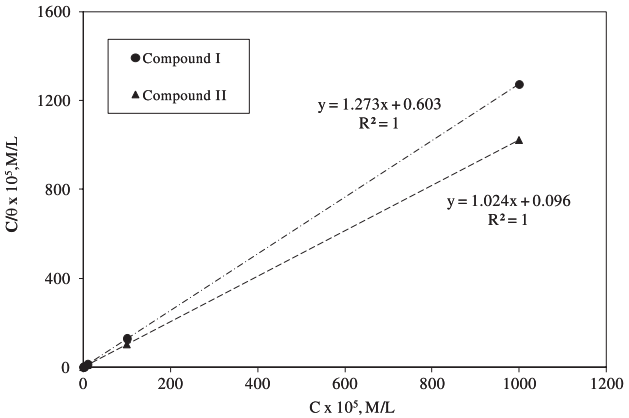

Fig. 5: Langmuir adsorption isotherm for the adsorption of organo-silicon compounds on carbon steel in 1 M H_2SO_4.

$$\theta = \frac{K_{ads} C_{inh}}{1 + K_{ads} C_{inh}} \tag{14}$$

$$\frac{C_{inh}}{\theta} = \frac{1}{K_{ads}} + C_{inh} \tag{15}$$

For investigated two compounds, straight lines were acquired with a R^2 values higher than 0.99, suggesting that the Langmuir model for adsorption fits very well with the experimental results. The slope value being very near to unity (1.025) in the case of compound II further establishes the cogency of the adsorption isotherm of Langmuir. Having said that, the Langmuir adsorption gradient deviates from unity for compound I (1.273), could be supposedly as a result of the interaction between adsorbed species on metal surface [30, 31], whereas ideal Langmuir isotherm is based on the assumption that the adsorbed species do not interact with each other.

3.4 Equilibrium constant of adsorption (K_{ads})

The equilibrium constant of adsorption (K_{ads}) is considered as an important factor to describe the vigor of the adsorption-desorption tendency of the inhibitor (adsorbate) on the metal surface (adsorbent). It was calculated from the reciprocal of the intercept of the linear representation with the unit of the slope as

reported in Figure 5. The obtained values of the adsorptive equilibrium constants (K_{ads}) are 165,590 and 1,042,000 M^{-1} for inhibitors I and II, respectively, as reported in Table 3. Distinctly, the great values of K_{ads} point out a vigorous adsorption of the synthesized compounds on the carbon steel surface in 1 M H_2SO_4 solution, hence better inhibition efficiency. That is to say, coordinated bonds were formed between the electron lone pairs and/or π-electrons of inhibitor molecule and the d-orbital of iron on the surface of steel, accordingly a stronger and more stable adsorbed layer was formed on the steel surface [32]. Another key point to remember is the higher value of K_{ads} for inhibitor II show stronger adsorption on the steel surface of carbon than inhibitor I which explain the high inhibition efficiency obtained for compound II.

3.5 Adsorption Gibbs free energy (ΔG^o_{ads})

Thermodynamically, the K_{ads} of the synthesized compounds on the carbon steel surface is joined to the free energy of adsorption (ΔG^o_{ads}) based on the next equation [33]:

$$\Delta G^o_{ads} = -RT \ln (55.5\, K_{ads}) \tag{16}$$

where, ΔG^o_{ads} is the Gibbs free energy of adsorption, T is the absolute temperature and K_{ads} is the equilibrium constant for the adsorption process and 55.5 is the molar concentration of water in solution. The addition of the synthesized inhibitors caused negative values of ΔG^o_{ads} which have been verified that these inhibitors were adsorbed spontaneously on the carbon steel surface. Prosaically, if ΔG^o_{ads} values equipped –20 kJ mol^{-1}, the adsorption is physical adsorption for the cause of the electrostatic interactions between the charged molecules and the charged steel surface, however about –40 kJ mol^{-1} were considered as chemical adsorption which is a result of charge sharing or a transfer from the inhibitor molecules to the steel surface to form a coordinate covalent bond [34–36]. In the current seeking, the calculated (ΔG^o_{ads}) values of compound I and compound II (Table 3) were –40.39 kJ mol^{-1} and –45.02 kJ mol^{-1}, respectively. Correspondingly, it was specified that the spontaneity of compounds adsorption on the metal surface with more approaching to chemical adsorption rather than the physical one at the studied temperature [37]. Notably, the presence of the lone sp^2 electron pairs existent on the N, S and/or O atoms of the inhibitor were involved in the formation of links with the d-orbital of iron atoms coupled with the displacement of water molecules from the metal surface, altogether chemical adsorption of the organo-silicon molecules takes place.

3.6 Surface morphology using SEM analysis

According to the electrochemical measurements it was realized that the surface film change occurs meantime the corrosion inhibition process, hence the morphological changes of the metal surface was examined by SEM after inundation in 1 M H_2SO_4 in the lack and occurrence of tested inhibitors and the micrographs obtained are revealed in Figure 6a–c. As be able to seen from Figure 6a, specimen dipped in 1.0 M H_2SO_4 electrolyte in the lack of inhibitor shows highly coarse surface and there are micro-holes on the eroded surface and some pets can be observed. It can be easily noticed that the metal dissolution created a damaged surface. Whilst, the presence of optimum concentration of inhibitors (I and II) quash the corrosion rate and consequently the surface spoilage has been extremely minified (Figure 6b,c), respectively, indicating that a protective inhibitor film was formed on the carbon steel surface which furnished abundant defense to carbon steel alloy versus metal deterioration.

3.7 EDX observations

With a view to obtain a datum about the composition of the exposed and protected carbon steel surface, EDX technique was employed. Figure 7a–c clarifies the results of EDX analysis. The diverse elements proportion weight content of the investigated carbon steel surface specified by EDX is reported in Table 4. The data shows that, the percentage weight content of Fe for C-steel dipped in 1.0 M H_2SO_4 electrolyte is 54.19%, while carbon steel dipped in a maximum concentration of compounds I and II are 15.69% and 11.1%, respectively.

Through Figure 7a–c, it is obvious that the bands of the carbon steel specimens in the inhibited solutions show low height Fe peaks, when compared with inhibitor free sample because of establishment of inhibitor layer on carbon steel surface. The EDX spectra of inhibited carbon steel contain some other signals like Si and S indicative that the inhibitor particles have been absorbed on the surface of the carbon steel.

3.8 XRD patterns analysis

For further investigation of the nature of carbon steel surface film, XRD analysis was accomplished after 24 h of immersion in the blank 1 M H_2SO_4 solution and in acidic solution containing the tested inhibitors. The results are presented in Figure 8, XRD pattern of the sample in the blank solution shows the crystalline

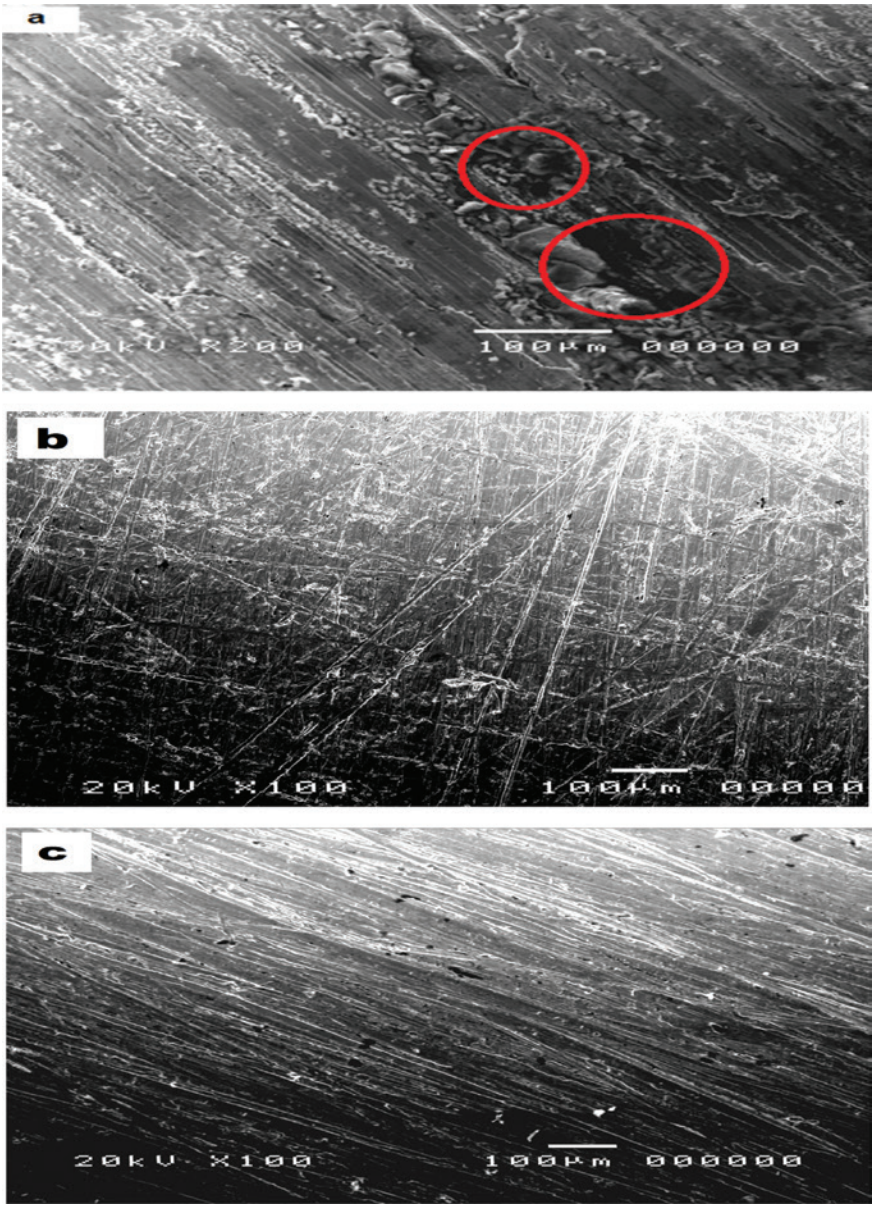

Fig. 6: SEM micrographs of carbon steel specimens in corrosive acidic electrolyte; (a) without inhibitors, (b) with compound I and (c) with compound II.

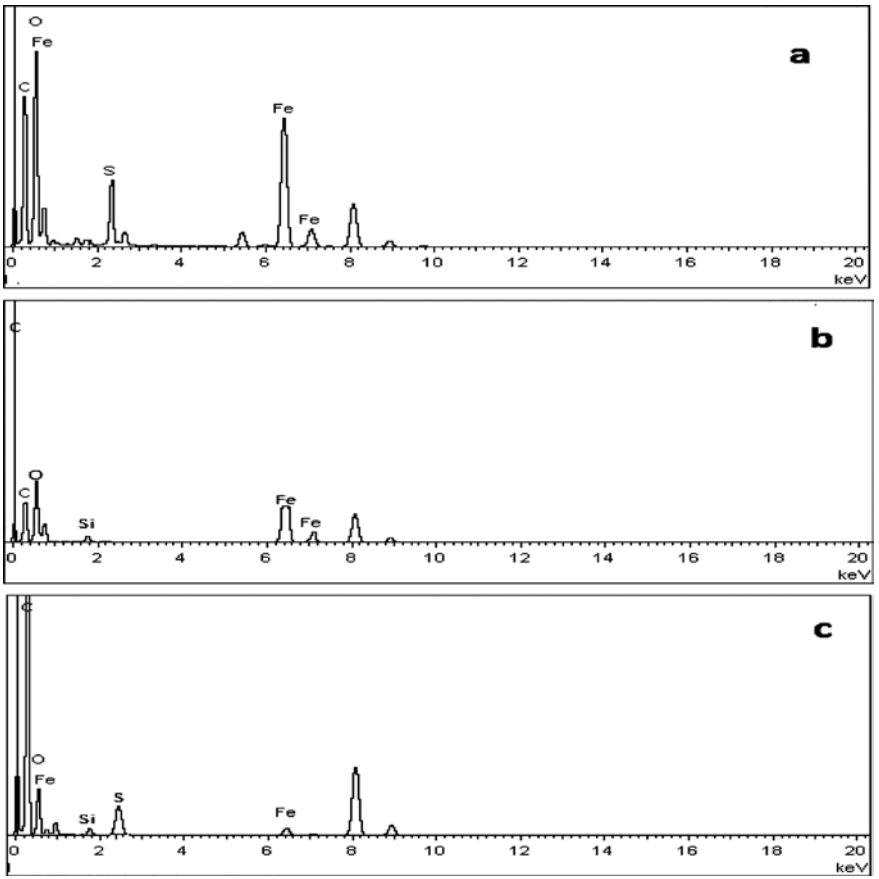

Fig. 7: EDX spectra of uninhibited and inhibited carbon steel surface after immersion for 24 h in (a) 1 M H_2SO_4, (b) 1 M H_2SO_4 + compound I and (c) 1 M H_2SO_4 + compound II.

character of the formed film as indicated from the sharp narrow peaks. Analysis of the blank pattern declares that, two main phases are detected as corrosion products, iron sulfate hydrate as dominating phase with maximum peak intensities of 100, 73.89, 69 and 52% at positions $2\theta = 19.89$, 16.29, 22.39 and 26.26, respectively, and the other identified secondary phase is iron oxide hydroxide in which its characteristics peaks are detected at positions $2\theta = 21.23$, 34.84 and 36.99 with intensities of 27, 33 and 30%, respectively. The XRD spectra for the alloy in the solution containing compounds I and II inhibitors do not show any identified crystalline phase and further more show the change of the film character into the amorphous nature. This qualitative change in the nature of the formed film could be attributed to that the original surface film composition has been changed by

Tab. 4: Percentage weight contents of elements for carbon steel (CS) obtained from EDX spectra analysis.

Sample	Fe (wt.%)	C (wt.%)	O (wt.%)	S (wt.%)	Si (wt.%)
CS in blank in H_2SO_4	54.19	13.6	19.56	12.65	–
CS in H_2SO_4 + compound I	15.69	49.8	33.39	–	1.12
CS in H_2SO_4 + compound II	11.1	51.31	33.14	3.2	1.25

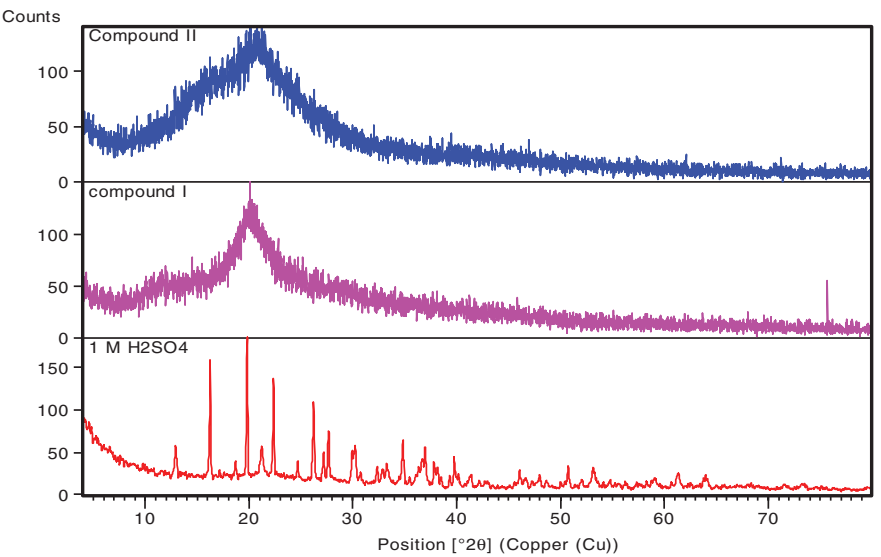

Fig. 8: XRD patterns of carbon steel alloy after immersion for 24 h in blank and inhibited 1 M H_2SO_4.

the organic inhibitor adsorption on carbon steel sample. This result confirms the efficiency of the studied inhibitors in controlling the protection of steel alloy from corrosion in 1 M H_2SO_4.

3.9 Computational quantum studies

In order to evaluate the influence of geometrical and electronic structural factors on the corrosion efficiency of inhibition of compound I and II and deduce the mechanism of adsorption occurring on the surface of the steel, quantum chemical studies were undertaken. The electronic and geometrical structures of the tested compounds were deduced through the maximum benefit of bond length,

bond angles and dihedral angles. Optimal Structures, highest occupied molecular orbital (HOMO), lowest unoccupied molecular orbital (LUMO), total electron density surface mapped with electrostatic potential (ESP), Mulliken charges and contour exemplification of electrostatic potential are shown in Figure 9. The calculations reveal that the top molecular orbital factor in the HOMO level might be characterized around one of the two eight membered rings those containing two O and one N atoms. So, this ring moiety was oriented towards the carbon steel surface and the adsorption may take place mainly through this ring moiety.

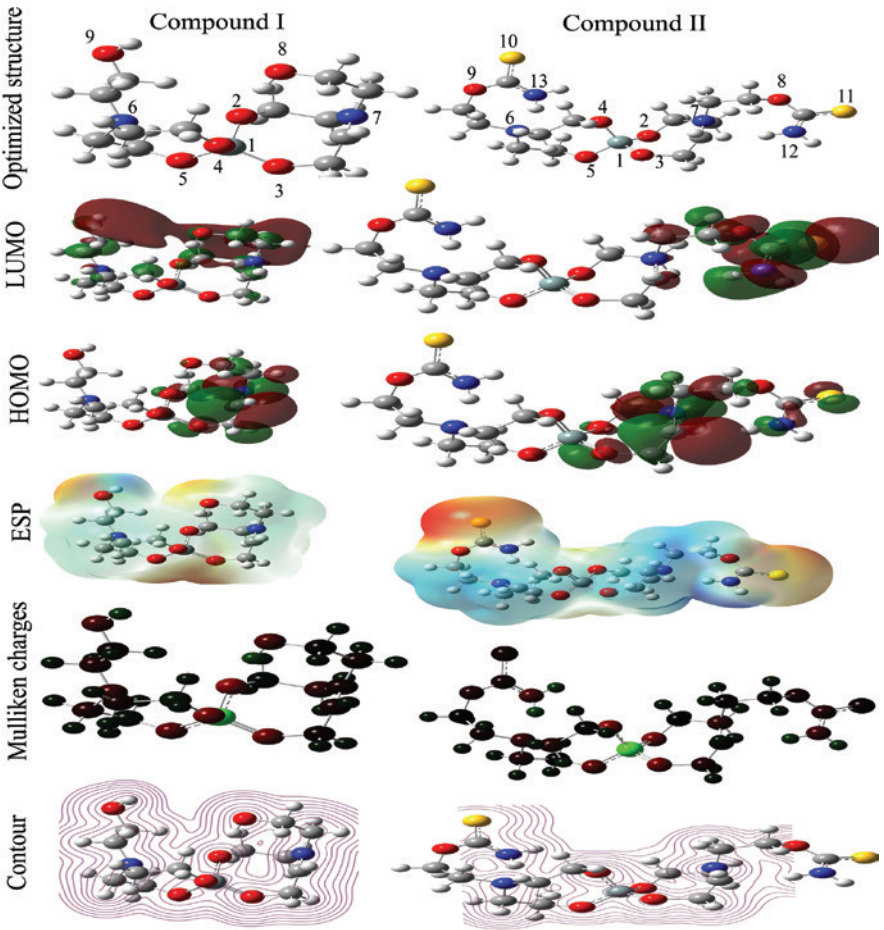

Fig. 9: Optimized structures, HOMO, LUMO, total electron density surface mapped with electrostatic potential, Mulliken charges values and contour representation of electrostatic potential for the investigated compounds.

Also, density of the electrostatic potential gives good information about the area that has additional negatively charged (colored by red) and other type of the positively charged atoms (colored by blue). Atoms containing negative charge can be considered as the area that will attack the steel surface. Moreover, it helped to anticipate sites available to receive protons.

The calculated bond distances and charge densities for heteroatoms of the tested compounds (I and II) are shown in Tables 5 and 6. The data in Table 5 utilizing DFT/B3LYP/6-311+G (d,p) showed that Si atom attached to four O atoms through tetrahedral structure with bond lengths vary from 1.64 to 1.67 Å, each two O atoms from the tetrahedral attached to four C atoms and one N atom forming eight membered alicyclic ring with bond lengths for C–N approximately 1.47 Å and there are no great differences in bond lengths between compound I and compound II for these atoms. In case of compound I, it has two terminal OH groups with a C–O bond length around 1.42 Å that had been slightly increased upon substitution to be around 1.44 Å for compound II. Compound II also has two S=C bonds that are the longest bond length with values equal to 1. 66 Å which may facilitate its adsorption on steel surface and so protect against corrosion. Compound II has two N–C bonds, which in conjugation with C=S and have the shortest bond length 1.36 Å.

Mullikan population analysis is used over a large area of research to evaluate the adsorption sites and its distribution over the corrosion inhibitors [38]. The calculated Mullikan charges data in Table 6 indicated that there is more than one active site as a result of the presence of more than one hetero atom and it is well known that as the atomic partial charges of the adsorbed center become more negative, as the atoms donate its electrons easily to the unoccupied d-orbital of the metal and hence adsorption occurs more easily. The calculation showed that Si atom acquires positive charge with values 2.021 and 1.886 e for compound I and compound II, respectively, using DFT/B3LYP/6-31+G (d,p) method, and with values 2.884 and 2.674 e for compound I and compound II, respectively, using HF/6-31+G (d,p) so it cannot act as adsorption center for inhibitors molecules. The calculation also showed that the other heteroatoms (O, N and S) bear negative charges and can act as adsorption centers. The four O atoms around Si have maximal negative charge in two investigated compounds for each values ranged from –0.6 to –0.8 e for compound I and compound II, using DFT/B3LYP/6-31+G (d,p) method. It is also found that the two N atoms of the eight membered rings have maximal negative charge for each values ranged from –0.13 to –0.40 e for compound I and compound II, using DFT/B3LYP/6-31+G (d,p) method. Two terminal O atoms in state of compound I acquire maximal negative charge, –0.517 and –0.514 e, while they have values of –0.181 and –0.233 in case of compound II using DFT/B3LYP/6-31+G (d,p) method. Compound II overcomes compound I by more four adsorption

Tab. 5: The calculated bond lengths for the investigated compounds.

Molecule	.Bond distance											
	Si1–O2	Si1–O3	Si1–O4	Si1–O5	C–N6	C–N7	C–O8	C–O9	C–S10	C–S11	C–N12	C–N13
DFT/B3LYP/6-31+G (d,p)												
Compound I	1.676	1.643	1.644	1.649	1.462	1.455	1.418	1.427	–	–	–	–
Compound II	1.645	1.643	1.655	1.647	1.475	1.459	1.442	1.446	1.663	1.661	1.360	1.354
HF/6-31+G (d,p)												
Compound I	1.642	1.623	1.619	1.624	1.454	1.447	1.397	1.404	–	–	–	–
Compound II	1.622	1.621	1.621	1.628	1.461	1.458	1.426	1.424	1.664	1.660	1.337	1.331
Semi-empirical/PM6												
Compound I	1.649	1.577	1.571	1.647	1.499	1.484	1.426	1.433	–	–	–	–
Compound II	1.636	1.548	1.567	1.655	1.495	1.486	1.456	1.457	1.662	1.655	1.363	1.358

Tab. 6: The calculated charge densities for the investigated compounds.

Molecule	.Net atomic charges												
	Si1	O2	O3	O4	O5	N6	N7	O8	O9	S10	S11	N12	N13
DFT/B3LYP/6-31+G (d,p)													
Compound I	2.021	−0.888	−0.740	−0.789	−0.624	−0.402	−0.139	−0.517	−0.514	–	–	–	–
Compound II	1.886	−0.734	−0.709	−0.749	−0.602	−0.375	−0.327	−0.181	−0.233	−0.130	−0.097	−0.401	−0.488
HF/6-31+G (d,p)													
Compound I	2.884	−1.111	−0.979	−1.116	−0.924	−0.422	−0.310	−0.629	−0.607	–	–	–	–
Compound II	2.674	−0.920	−1.002	−0.949	−0.953	−0.404	−0.394	−0.345	−0.355	−0.341	−0.329	−0.608	−0.604
Semi-empirical/PM6													
Compound I	0.386	−0.408	−0.441	−0.453	−0.418	−0.113	−0.315	−0.551	−0.567	–	–	–	–
Compound II	0.369	−0.450	−0.391	−0.402	−0.442	−0.334	−0.157	−0.356	−0.360	−0.538	−0.504	−0.521	−0.511

centers represented by two S atoms and two N atoms which explain the high inhibition efficiency of compound II in comparison to compound I. The values of atomic charges on S atoms are −0.130 and −0.097 e but they are −0.401 and −0.488 for the other two N atoms in compound II using DFT/B3LYP/6-31+G (d,p) method.

The computational parameters resulted from the quantum chemical calculations which are responsible for the inhibition efficiency of inhibitors, such as the energies of highest occupied molecular orbital (E_{HOMO}), energy of lowest unoccupied molecular orbital (E_{LUMO}), the separation energy ($E_{LUMO} - E_{HOMO}$), ΔE, representing the function of reactivity, separation energy for the electronic back-donation, $\Delta E_{Back\text{-}donation}$, global hardness, η, Softness, σ, global electrophilicity, ω, Absolute electro negativity, X, fraction of electron transferred, ΔN, maximum amount of electronic charge that an electrophile may accept from its environment, ΔN_{max}, dipole moment, DM, summation of the total negative charges on atoms over the skeleton of the molecule (TNC), total energy (TE), and molecular volumes of molecule (MV), are collected in Table 7.

Frontier molecular orbitals (HOMO and LUMO) of chemical compounds act an essential role in clarifying their reactivity and hence adsorption on carbon steel surface takes place. Interpretation of the interplay between HOMO in addition to LOMO levels of reacting species is attributed to the occurrence of a chemical reaction or the transfer of one or more electrons. The higher value of E_{HOMO}, the better is its capability to give electrons to the appropriate acceptor leading to better adsorption and inhibition efficiency [39]. By comparing compound I and compound II on basis of E_{HOMO}, we can notice that compound II which ranks first in inhibition efficiency values, has the least negative value (i.e. the highest) E_{HOMO} with values of −5.661, −8.409 and −7.938 eV using DFT/B3LYP/6-31+G (d,p), HF 6-31+G (d,p) and PM6 techniques, respectively. On the other side compound II which ranks first in inhibition efficiency values, gave the highest negative value (i.e. the lowest) of E_{HOMO} with values of −6.123, −9.983 and −9.173 eV using DFT/B3LYP/6-31+G (d,p), HF 6-31+G (d,p) and PM6 techniques, respectively, these data agree well with that obtained from the experimental results. The energy of the LUMO can be considered as the susceptibility of molecule towards attacking by nucleophile and consequently receiving electrons. Good corrosion inhibitors can donate electrons to free orbital of the steel and also can get electrons from the steel, so as E_{LUMO} decreases, the capability of the inhibitor compounds to gain electrons increases [40]. The calculations showed that compound II has the lowest value of E_{LUMO} which advocate its high efficiency of inhibition. Separation energy ΔE, $E_{LUMO} - E_{HOMO}$, is a remarkable factor as reactivity index of the investigated compounds across the adsorption on the surface of steel. As ΔE values drops, the reactivity of inhibitor compound and so the ability of adsorption on the surface of steel increases subsequent in enhancing the efficiency of inhibition. Data proved that tested compound II inhibitor

Tab. 7: The calculated quantum chemical parameters in eV for the studied inhibitors.

Molecule	E_{HOMO} (eV)	E_{LUMO} (eV)	ΔE (eV)	$\Delta E_{Back\text{-}donation}$ (eV)	DM (D)	TE (eV)	MV (cm^3/mol)	TNC (e)	η (eV)	σ (eV^{-1})	ω (eV)	X (eV)	ΔN (e)	ΔN_{max} (e)	IE[a] (%)
DFT/B3LYP/6-311G+(d,p)															
Compound I	−6.123	−0.993	5.13	−0.64	1.201	−35967.1	197.08	−6.224	2.565	0.389	2.46	3.558	0.670	1.387	79
Compound II	−5.661	−2.237	3.42	−0.42	8.558	−62703.7	288.58	−6.751	1.712	0.584	4.55	3.949	0.890	2.306	98
HF/6-311G+(d,p)															
Compound I	−9.983	1.594	11.57	−1.44	1.097	−35785.2	274.67	−7.029	5.789	0.172	1.51	4.19	0.242	0.724	79
Compound II	−8.409	1.1569	9.56	−1.19	8.974	−62454.2	275.65	−8.057	4.782	0.209	1.37	3.62	0.352	0.758	98
Semiempirical/PM6															
Compound I	−9.173	−1.189	7.984	−0.99	2.284	−14.2	381.71	−4.440	3.992	0.250	3.36	5.18	0.227	1.297	79
Compound II	−7.938	−0.354	7.584	−0.94	11.442	−12.9	430.69	−6.397	3.792	0.263	2.26	4.14	0.376	1.093	98

has lower ΔE values, 3.42, 9.56 and 7.584 eV (using DFT/B3LYP/6-31+G (d,p), HF 6-31+G (d,p) and PM6 techniques, respectively) than that obtained by compound I inhibitor, thus compound II has higher reactivity than compound I thus leading to greater efficiency of inhibition. Dipole moment (DM) is an index of the electronic distribution in compounds. It is indication for polarity in a chemical bond; a large value dipole moment value denotes polar nature for the investigated compound, while a small dipole moment value denotes nonpolar nature for the investigated compound [41]. Inhibitors with large value of dipole moment have the capability to form strong dipole–dipole interactions with steel surface, leading to greater efficiency of inhibition [42]. Results recorded in Table 7 illustration that both compound I and compound II have significant dipole moments, which assist their adsorption on the surface of steel, and the tendency of DM values also shows that the explanation of increased efficiency of inhibition is due to the dipole moment increase of the investigated compounds. Molecular volume (MV), which provides us with evidence around the contact area among the investigated compounds and the surface of steel, it was as well assigned to the studied compounds. The efficiency of inhibition of chemical compounds increase as their volume increases which is a results of increasing the contact surface between compounds and steel resulting in more surface coverage [43]. According to the obtained results, molecular volume is higher in compound II than compound I. This is agreeing well with experimental data.

The number of electrons transferred (ΔN), was also calculated. However, the phrase "The ability to donate electrons is more appropriate than the number of electron transfers" because the absolute values did not express the real values [44]. If $\Delta N < 3.6$, the ability of molecules for donating electrons to steel surface increases by increasing ΔN. According to values of ΔN, the order of the investigated compounds will be compound II > compound I, because the calculations indicate that compound II has the highest ΔN values (0.890, 0.352 and 0.376 e) where, compound I has the lowest ΔN values (0.670, 0.242 and 0.227 e) in DFT/B3LYP/6-31+G (d,p), HF 6-31+G (d,p) and PM6 techniques, respectively. The maximum number of electrons transferred (ΔN_{max}) can be determined by following equation $\Delta N_{max} = \chi/(2\,\eta)$ [45]. The results proved that (ΔN_{max}) greater than before via the identical ranking attained from the results of experiments that indicate that the order of inhibition efficiency is compound II > compound I.

The locales of the ionic reaction might be assessed from the net charges of atoms on a molecule, as the inhibitor molecules adsorb on the surface of steel through negative centers, thus the total negative charge (TNC) has been determined. When TNC increases, the efficiency of inhibition increases. It is clear from calculations that compound II has the top values of TNC equal to −6.751, −8.057

and −6.397 e in DFT/B3LYP/6-31+G (d,p), HF 6-31+G (d,p) and PM6 techniques, respectively. These results indicate the same order of reactivity (compound II > compound I).

The interplay between inhibitor and steel surface can be discussed through the conditions of the HSAB (strong-soft-acid-base) and the frontier-controlled interaction principals. It is suggested that strong acids prefer to coordinate to strong bases and soft acids prefer to coordinate to soft bases. It is well known that strong molecules have a high HOMO–LUMO gap and soft molecules have a small HOMO–LUMO gap [46]. Soft base inhibitors are extra efficient for the metals for the reason that the steel atoms are considered as soft acids. Calculations revealed that compound II has the greatest σ with values equal to 0.584, 0.209 and 0.263 eV^{-1} in DFT/B3LYP/6-31+G (d,p), HF 6-31+G (d,p) and PM6 techniques, respectively, and so it showed the greatest efficiency of inhibition. As well as found that the compound I has the uppermost hardness η with values equal to 2.565, 5.789 and 3.992 eV in DFT/B3LYP/6-31+G (d,p), HF 6-31+G (d,p) and PM6 techniques, respectively, which demonstrate that it has the minimal reactivity and accordingly the lowest inhibition efficiency.

Electronic back-donation process can control the interaction between the inhibitor molecule and the metal surface referring to the charge transfer model for donation and back donation of charges proposed by Gomez et al. [47]. Inspection of Table 7 leads us to the conclusion that, the trend of the $\Delta E_{Back\text{-}donation}$ is in accordance with the inhibition efficiency order obtained from experimental data (compound II > compound I).

3.10 Molecular dynamics simulations

To understand the adsorption mechanism of the investigated compounds on steel surface molecular dynamic emulation were done on a system consisting of the surface of steel and inhibitor molecules. Inhibitory compounds were optimized first by forcite geometry optimization prior placing them on the iron surface. Figure 10. Appearances the optimization energy curves for the inhibitors molecules.

Adsorption calculations were done using adsorption locator tool on investigated compounds/iron surface to deduce the minimal energy for the entire system. Overall energy, average overall energy, van der Waals energy, electrostatic energy and intramolecular energy for compound II (as an example)/Fe (110) surface are presented in Figure 11. The results are displayed and described in Table 8. The parameters existing in Table 8 comprise the total energy, adsorption energy (rigid adsorption energy and the deformation energy) and the differential adsorption

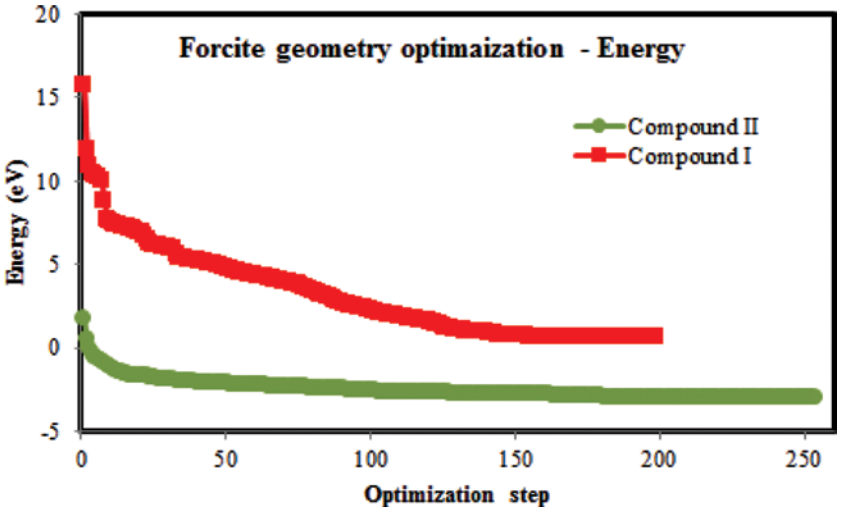

Fig. 10: Optimization energy curves for the studied molecules before putting them on the metal surface.

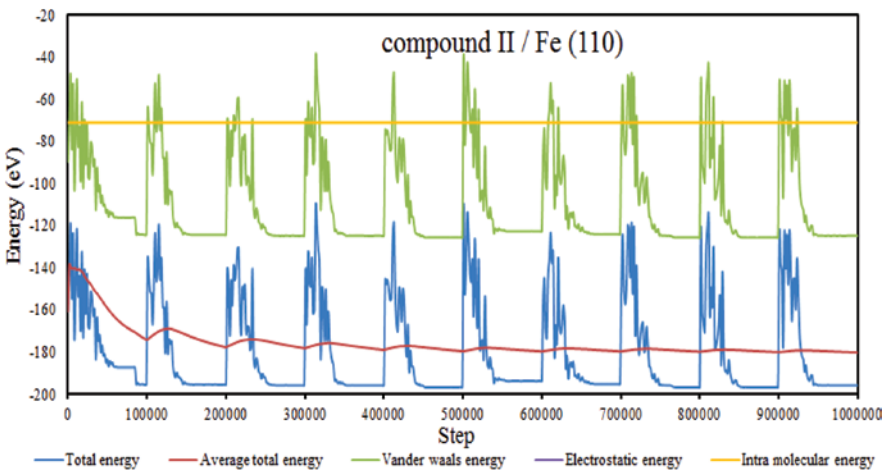

Fig. 11: Total energy distribution for compound II/Fe (110) system during energy optimization process.

energy [48]. The data showed that the adsorption energies of the two investigated compounds have negative values which show their ability for adsorption on Fe (110) surface. The binding energies values showed that compound II has a higher

Tab. 8: Outputs and descriptors calculated by the simulation for the adsorption of the inhibitors on Fe (110) surfaces.

Inhibitors	Total energy (eV)	Adsorption energy (eV)	Rigid adsorption energy (eV)	Deformation energy (eV)	(dE_{ads}/dNi) (eV)	Binding energy (eV)	IE (%)
Compound I	−6.159	−6.779	−6.725	−0.0529	−6.779	6.779	79
Compound II	−10.784	−7.703	−8.005	0.3013	−7.703	7.703	98

binding energy to Fe (110) surface and so higher inhibition efficiency than compound I. The binding energy of the investigated compounds is in the order: compound II > compound I.

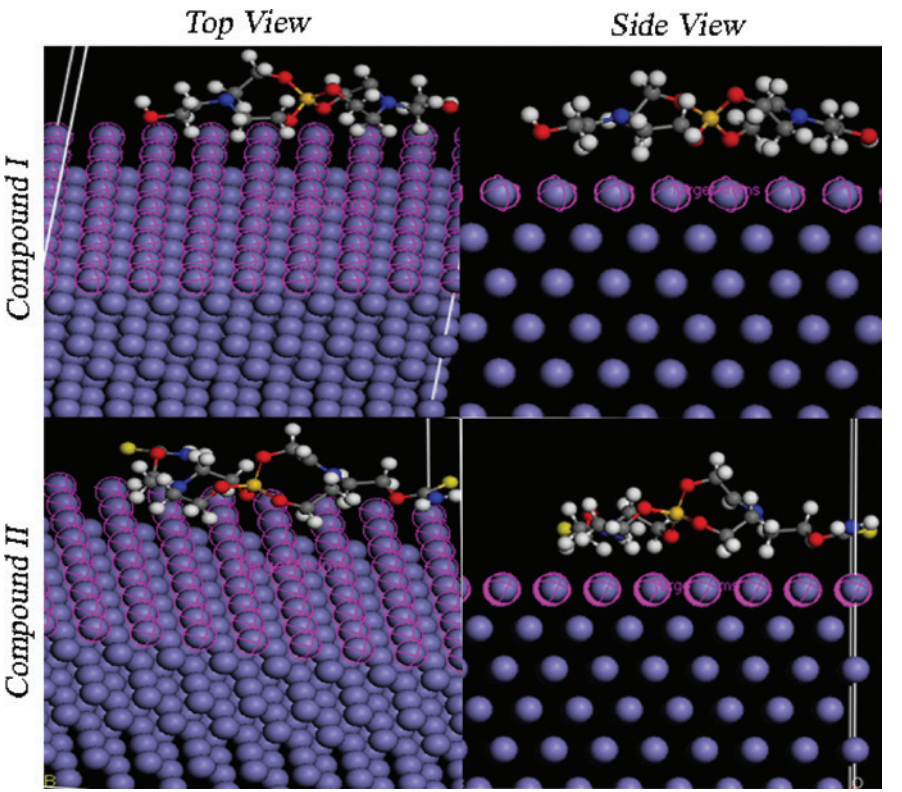

Fig. 12: Molecular simulations for the most favorable modes of adsorption obtained for the investigated inhibitors on Fe (110) surface, side and top view.

The geometrical structures of investigated compounds on Fe (110) surface (both top and side views) are shown in Figure 11. The studied compounds have lone pairs of electrons on the S, O and N atoms. So they are capable of providing electrons to the empty d-orbital of steel surface and forming a stable coordination bond. Figure 12 revealed that the utilized compounds can be adsorbed on the steel surface through the eight membered alicyclic rings. In presented case, most of the steel surface could be protected with the investigated compounds molecules, making an obstruction between the surface of the steel and the acid corrosive solution and hence protecting it from corrosion [49].

4 Conclusion

The following conclusions are achieved according to the results gained from the performed experimental data and the quantum studies:

1. The synthesized organo-silicon compounds were acting as effective corrosion inhibitors against carbon steel in 1 M H_2SO_4.
2. The application compounds were contained the siloxane group, which gives them stability during application and the more adsorption on the surface of the metals.
3. The adsorption mode of these compounds on steel surface is mixed physical and chemical adsorptions obeying Langmuir adsorption isotherm.
4. The good inhibiting ability of the investigated inhibitors was upheld using surface analyses such as SEM, EDX and XRD.
5. A good correlation between quantum chemical parameters and the inhibition efficiencies of these compounds was confirmed by quantum chemical study.
6. The molecular dynamics emulation data proved that investigated compounds have the ability to adsorb on steel surface over and done with both the donation of the π-charge of the two eight membered alicyclic rings and the unshared pair of electrons of the heteroatom.

Acknowledgment: This article was supported by the Egyptian Petroleum Research Institute (EPRI), Nasr City, P.B. 11727, Cairo, Egypt. The authors are greatly thankful to (EPRI) for its support.

References

1. A. Hamdy, N. S. El-Gendy, Egypt J. Petrol. **22** (2013) 17.
2. H. M. Abd El-Lateef, M. Ismael, A. H. Tantawy, Z. Phys. Chem. **230** (2016) 1111.

3. S. S. Abd El-Rehim, H. H. Hassan, M. A. M. Deyab, A. Abd El Moneim, Z. Phys. Chem. **230** (2016) 67.
4. S. S. Abd El-Rehim, M. A. Deyab, H. H. Hassan, A. M. Shaltot, Z. Phys. Chem. **231** (2017) 1573.
5. S. S. Abd El-Rehim, M. A. M. Deyab, H. H. Hassan, A. A. A. Ibrahim, Z. Phys. Chem. **230** (2016) 1641.
6. F. E.-T. Heakal, M. M. Osman, M. A. Deyab, A. E. Elkholy, Z. Phys. Chem. **232** (2017) 13.
7. M. A. Deyab, S. S. A. El-Rehim, H. H. Hassan, A. A. El-Moneim, Z. Phys. Chem. **231** (2017) 1141.
8. T. O. Siyanbola, K. Sasidhar, B. Anjaneyulu, K. P. Kumar, B. V. S. K. Rao, N. Ramanuj, O. Olaofe, E. T. Akintayo, K. V. S. N. Raju, J. Mater. Sci. **48** (2013) 8215.
9. S. Hejazi, S. H. Mohajernia, M. H. Moayed, A. Davoodi, M. Rahimizadeh, M. Momeni, A. Eslami, A. Shiri, A. Kosari, J. Ind. Eng. Chem. **25** (2015) 112.
10. K. Zakaria, A. Hamdy, M. A. Abbas, O. M. Abo-Elenien, J. Taiwan Inst. Chem. Eng. **65** (2016) 530.
11. M. A. Bedair, S. A. Soliman, M. S. Metwally, J. Ind. Eng. Chem. **41** (2016) 10.
12. M. A. Bedair, J. Mol. Liq. **219** (2016) 128.
13. A. D. Becke, Phys. Rev. **38** (1988) 3098.
14. A. D. Becke, J. Chem. Phys. **98** (1993) 5648.
15. C. T. Lee, W. Yang, R. G. Parr, Phys. Rev. **37** (1988) 785.
16. J. S. Dewar, E. G. Zoebisch, E. H. Healy, J. P. Stewart, J. Am. Chem. Soc. **107** (1985) 3902.
17. Gaussian 09, Revision A.02, M. J. Frisch, G. W. Trucks, H. B. Schlegel, G. E. Scuseria, M. A. Robb, J. R. Cheeseman, G. Scalmani, V. Barone, B. Mennucci, G. A. Petersson, H. Nakatsuji, M. Caricato, X. Li, H. P. Hratchian, A. F. Izmaylov, J. Bloino, G. Zheng, J. L. Sonnenberg, M. Hada, M. Ehara, K. Toyota, R. Fukuda, J. Hasegawa, M. Ishida, T. Nakajima, Y. Honda, O. Kitao, H. Nakai, T. Vreven, J. A. Montgomery, Jr., J. E. Peralta, F. Ogliaro, M. Bearpark, J. J. Heyd, E. Brothers, K. N. Kudin, V. N. Staroverov, R. Kobayashi, J. Normand, K. Raghavachari, A. Rendell, J. C. Burant, S. S. Iyengar, J. Tomasi, M. Cossi, N. Rega, J. M. Millam, M. Klene, J. E. Knox, J. B. Cross, V. Bakken, C. Adamo, J. Jaramillo, R. Gomperts, R. E. Stratmann, O. Yazyev, A. J. Austin, R. Cammi, C. Pomelli, J. W. Ochterski, R. L. Martin, K. Morokuma, V. G. Zakrzewski, G. A. Voth, P. Salvador, J. J. Dannenberg, S. Dapprich, A. D. Daniels, O. Farkas, J. B. Foresman, J. V. Ortiz, J. Cioslowski, D. J. Fox, Gaussian, Inc., Wallingford, CT (2009).
18. R. G. Parr, R. G. Pearson, J. Am. Chem. Soc. **105** (1983) 7512.
19. S. Martinez, Mater. Chem. Phys. **77** (2002) 97.
20. Y. Sasikumar, A. S. Adekunle, L. O. Olasunkanmi, I. Bahadur, R. Baskar, M. M. Kabanda, I. B. Obot, E. E. Ebenso, J. Mol. Liq. **211** (2015) 105.
21. S. Satoh, H. Fujimoto, H. Kobayashi, J. Phys. Chem. B **110** (2006) 4846.
22. L. Guo, S. Zhu, S. Zhang, J. Ind. Eng. Chem. **24** (2015) 174.
23. S. S. Mahmoud, J. Mater. Sci. **42** (2007) 989.
24. A. A. Farag, W. Ahmed, K. Zakaria, I. M. Nassar, Int. J. Sci. Res. **3** (2014) 870.
25. K. Zakaria, N. A. Negm, E. A. Khamis, E. Badr, J. Taiwan, Inst. Chem. Eng. **61** (2016) 316.
26. E. E. Oguzie, C. E. Ogukwe, J. N. Ogbulie, F. C. Nwanebu, C. B. Adindu, I. O. Udeze, K. L. Oguzie, F. C. Eze, J. Mater. Sci. **47** (2012) 3592.
27. M. Behpour, S. M. Ghoreishi, A. Gandomi-Niasar, N. Soltani, M. Salavati-Niasari, J. Mater. Sci. **44** (2009) 2444.
28. M. Abd El-Raouf, O. E. El-Azabawy, R. E. El-Azabawy, Egypt J. Petrol. **24** (2015) 233.

29. E. M. S. Azzam, M. A. Hegazy, N. G. Kandil, A. M. Badawi, R. M. Sami, Egypt J. Petrol. **24** (2015) 493.
30. A. S. Fouda, M. N. H. Moussa, H. A. Mostafa, Korros (Dresden). **18** (1987) 28.
31. A. A. Abdel-Azim, L. A. Shalaby, H. Abbas, Corros. Sci. **14** (1974) 21.
32. O. Benali, L. Larabi, S. M. Mekelleche, Y. Harek, J. Mater. Sci. **41** (2006) 7064.
33. O. A. Abdullatef, Egypt J. Petrol. **24** (2015) 505.
34. A. I. Adawy, M. A. Abbas, K. Zakaria, Res. Chem. Intermed. **42** (2016) 3385.
35. M. Yadav, S. Kumar, R. R. Sinha, S. Kumar, J. Dispers. Sci. Technol. **35** (2014) 1751.
36. K. I. Kabel, K. Zakaria, M. A. Abbas, E. A. Khamis, J. Ind. Eng. Chem. **23** (2015) 57.
37. M. J. Bahrami, S. M. A. Hosseini, P. Pilvar, Corros. Sci. **52** (2010) 2793.
38. O. K. Abiola, J. O. E. Otaigbe, O. J. Kio, Corros. Sci. **51** (2009) 1879.
39. M. B. Sabeel, C. W. Anthony, J. P. Ron, A. Sreekanth, Polyhedron **109** (2016) 7.
40. M. M. Ihebrodike, C. N. Michael, B. O. Kelechukwu, A. N. Lebe, A. C. Maduabuchi, C. E. Francis, E. O. Emeka, J. Mater. Sci. **47** (2012) 2559.
41. X. W. Zheng, S. T. Zhang, W. P. Li, M. Gong, L. L. Yin, Corros. Sci. **95** (2015) 168.
42. S. John, A. Joseph, RSC Adv. **2** (2012) 9944.
43. A. A. Nazeer, N. K. Allam, A. S. Fouda, E. A. Ashour, Mater. Chem. Phys. **136** (2012) 1.
44. F. Jia-jun, L. Su-ning, W. Ying, L. Xiao-dong, L. Lu-de, J. Mater. Sci. **46** (2011) 3550.
45. P. Geerlings, F. D. Proft, W. Langenaeker, Chem. Rev. **103** (2003) 1793.
46. P. R. Roberge, Handbook of Corrosion Engineering, McGraw-Hill, New York (2000).
47. B. Gomez, N. V. Likhanova, M. A. Dominguez-Aguilar, R. V. A. Martinez-Palou, J. Gasquez, J. Phys. Chem. **110** (2006) 8928.
48. K. F. Khaled, Electrochim. Acta **55** (2010) 5375.
49. A. I. Adawya, M. A. Abbasb, K. Zakariac, Pet. Sci. Technol. **33** (2015) 1348.